
AMERICAN REVOLUTION BICENTENNIAL 1776-1976

NBSIR 74-442

High Temperature Slow Crack Growth in Ceramic Materials

A. G. Evans

Inorganic Materials Division
Institute for Materials Research
National Bureau of Standards
Washington, D. C. 20234

February 1974

Interim Report for Period September 1, 1973 – January 31, 1974

Prepared for
United States Air Force
Air Force Systems Command
HQ 4950th Test Wing, 4950/PMMA
Wright-Patterson AFB, Ohio 45433
Delivery Order F 33615-73-M-6501

NBSIR 74-442

HIGH TEMPERATURE SLOW CRACK GROWTH IN CERAMIC MATERIALS

A. G. Evans

Inorganic Materials Division
Institute for Materials Research
National Bureau of Standards
Washington, D. C. 20234

February 1974

Interim Report for Period September 1, 1973 – January 31, 1974

Also to be published in Proceedings of Conference on Ceramics for High Performance Applications, Hyannis, Mass., Nov. 13–16, 1973.

Prepared for
United States Air Force
Air Force Systems Command
HQ 4950th Test Wing, 4950/PMMA
Wright-Patterson AFB, Ohio 45433
Delivery Order F 33615-73-M-6501

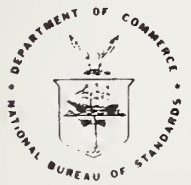

U. S. DEPARTMENT OF COMMERCE, Frederick B. Dent, Secretary

NATIONAL BUREAU OF STANDARDS, Richard W. Roberts, Director

ABSTRACT

High temperature slow crack growth processes in several ceramic materials are examined under static and cyclic loading conditions. Data obtained at temperatures up to 1400°C are used for purposes of failure prediction and for analysis of the slow crack growth phenomena. It is shown that purity plays a major role in slow crack growth resistance, particularly in the hot pressed materials, and that cycling in the low frequency regime does not significantly increase the rate of slow crack growth. The slow crack growth mechanisms appear to be primarily plasticity related. Two semi-quantitative mechanisms are presented, one due to dislocation motion and the other due to grain boundary sliding.

1. INTRODUCTION

Slow crack growth is a widespread phenomenon and several reviews of this extensive topic have appeared in the recent literature.[1,2] The content of this paper is thus restricted primarily to the more recent developments; especially in slow crack growth at elevated temperatures. High temperature slow crack growth occurs in a number of ceramic systems; e.g., silicon nitride above 1000°C,[3,4] alumina above 800°C;[5] and since this temperature regime is a critical one for the structural applications of primary interest at this symposium, it seems appropriate to address this problem in some detail.

First, the fracture mechanics techniques for evaluating slow crack growth at high temperatures are described, for both static and cyclic loading conditions. Then, data obtained for a variety of materials are described. Since purity is one of the most important microstructural variables affecting high temperature slow crack growth, impurity effects are examined in a controlled way. Then some conclusions are reached concerning the requisite types and distributions of impurity for good slow crack growth resistance.

The primary role of slow crack growth studies is the application of the slow crack growth data to failure prediction.[6] Hence, the analytical procedures for developing the time dependent failure parameters from slow crack growth data are examined. Then the materials with the greatest potential for effective structural use at very high temperatures are identified and the possibilities for further

improvements discussed.

Finally, the data are used to discuss the processes that lead to slow crack growth in ceramic systems at high temperatures. We identify two fundamental processes; crack propagation due to grain boundary sliding, and crack propagation due to dislocation activity. Semi-quantitative models for both processes are developed and correlated with data for silicon nitride, silicon carbide, and alumina.

2. TECHNIQUES

The fracture mechanics specimen which has the greatest versatility for effective slow crack growth rate measurements at elevated temperatures is the double torsion specimen[7] (Fig. 1). This specimen can be most easily used for slow crack growth rate measurements under fixed grip conditions;[8,9] where the crack growth rate is determined directly by the rate of load relaxation. This approach is only effective when crack growth is not accompanied by gross plasticity, and unfortunately, several of the important structural ceramic materials exhibit gross plasticity under typical operating conditions. But, the specimen can be used in a different mode,[4] fixed displacement rate, to obtain valid slow crack growth rate measurements when gross plasticity, of the linear viscoelastic type, is occurring. In this mode a load plateau is observed when crack propagation commences, as shown in Fig. 2, and the crack growth rate, V, is related to the plateau load, P_p, by:[4]

$$V = \frac{\dot{y}_{el}}{BP_p} \qquad (1)$$

where $\dot{y}_{el}$ is the elastic displacement rate at the loading positions (given by the applied displacement rate if the plastic displacements are small) and B is a constant which can be determined either empirically[2] or analytically.[8,4] The corresponding value for the stress intensity factor K_I is:[8]

$$K_I = pW_m \left[\frac{3(1+\nu)}{Wd^3 d_n}\right] \qquad (2)$$

where ν is Poisson's ratio and W_m, W, d and d_n are specimen dimensions, shown in Fig. 1. When non-plateau behavior is observed, substantial plastic displacements are generally occurring,[4] and valid parameters can no longer be obtained from Eq. (1), because $\dot{y}_{el}$ is indeterminate. This limits the velocity range which gives valid fracture mechanics parameters; for example, in silicon nitride at 1400°C, plateau behavior is only observed at velocities larger than 10^{-6} cm/sec. But the velocity regime below 10^{-6} cm/sec is the crucial one for failure prediction, and it is clear that further modifications are required to extend the capabilities of the technique.

A suitable modification entails crack growth measurements at constant load, where the crack growth rate is obtained from <u>direct</u> measurement of the extent of the crack tip displacement, Δa, in a predetermined time interval, Δt, using a fluorescent dye penetrant to indicate the position of the crack

tip.* Since the crack moves essentially at constant velocity in this mode, the velocity is determined directly by, $V = \Delta a/\Delta t$. The stress intensity factor must still, however, be determined from the load. There is some concern, therefore, that the substantial plastic displacements may affect the relation between load and stress intensity factor, given in Eq. (2), even for linearly viscoelastic materials. Analysis and experimentation[10] have shown that the stress intensity factor, after plastic deformation of the loading arms, is less than the value given by Eq. (2): but that the diminution is rather small, even for plastic displacements several times the specimen thickness; e.g., a maximum correction of 20% is required for a plastic displacement three times the specimen thickness. The effect of plastic displacements on the stress intensity factor, load relation is not therefore a crucial consideration for fracture mechanics measurements at low crack velocity, and we feel that the detailed evaluation of a correction factor is not merited at this time. We shall thus use the standard relation (Eq. 2) to evaluate the stress intensity factor. (We also assess the validity of

---

* For side-grooved double torsion specimens, this is achieved by inserting the specimen in the test fixture with the side groove along the top. Then the furthest extension of the crack is clearly indicated on the bottom face of the specimen. This inversion of the specimen from normal usage[6,7,8] has no effect on the crack propagation parameters.

this approximation for each specimen by obtaining the critical load for crack propagation at room temperature--which can be equated to K_{IC}--after the high temperature measurements have been completed.)

The same specimen configuration can be used to determine crack propagation rates under cyclic loading conditions.[11] Cycling is conducted between two fixed loads, p_1 and p_2, and the amount of crack growth that accompanies the imposed cycle is measured. Again the crack growth rate is determined from direct measurement of the crack tip displacement in a predetermined time interval, and the loads p_1 and p_2 give the corresponding stress intensity factor range, $2\Delta K_I$. The crack growth rate can then be plotted as a function of the average stress intensity factor $(K_I)_{av}$ for various ΔK_I, and compared with the "static" slow crack growth rates, using an analysis developed by Evans and Fuller.[11]

3. SLOW CRACK GROWTH RATE MEASUREMENTS

Measurements of slow crack growth rate have been obtained for a range of silicon nitrides,[4,10,12] silicon carbides,[10] and aluminas.[5] The most extensive work has been performed on the silicon nitrides and this is examined first.

3.1 Silicon Nitride

The temperature dependence of the slow crack growth rate obtained using the constant displacement rate approach[4] is shown in Fig. 3. We note two distinct regions of behavior, denoted regions A and B. In region A (at low velocity) the crack growth rate increases with increase in temperature (for a given stress intensity factor); whereas in region B,

the inverse occurs. The region A behavior can be analyzed in terms of a conventional rate process to obtain an apparent activation energy for slow crack growth,[4] ∿ 200 Kcal/mol.

More extensive data obtained at 1400°C,* using the constant load approach for low velocity measurements,[10] are shown in Figs. 4 and 5. Interestingly enough, when the data are plotted using a linear stress intensity axis (Fig. 4), there is a suggestion of a slow crack growth limit; but when plotted on a logarithmic K axis (Fig. 5), a good linear fit is obtained over the entire range. A good representation of the slow crack growth data is thus;[6]

$$V = AK_I^n \tag{3}$$

where A and n are constants for a given temperature. This we will find later is very convenient analytically; but, as yet, we find no fundamental reason for predicting this type of relation for a rate-controlled process. It is also noted that the incorporation of the lower velocity data (compared

---

* The most critical temperature for high temperature applications, such as in gas turbines.

to Fig. 3) permits more precise evaluation of the exponent, n. A least squares fit of the data for the same 'standard' material indicates that n (at 1400°C) is 6 ± 1.

The orientation dependence of the crack growth rate has also been evaluated[10,12] at 1400°C as shown in Fig. 6. It is apparent that the crack propagation rates on planes containing the hot-pressing direction are marginally larger than on the planes orthogonal to the hot-pressing direction, consistent with the orientation dependence of the strength noted by Lange.[3] All subsequent crack propagation rate measurements performed on research grade silicon nitrides* are conducted on the "strong" (orthogonal) planes because specimens of the other orientation cannot be prepared from the relatively small compacts.

Crack propagation rates obtained for a range of research grade silicon nitrides are also plotted in Figs. 4 and 5. These materials are characterized by different total impurity contents and/or different spatial and size distributions of essentially the same impurities. The classification is summarized in Table I. It is obvious that the higher purity materials (characteristically those with a low calcium content) exhibit substantially superior slow crack growth behavior. For example, the slow crack growth rate in the critical low velocity regime can be reduced by more

---

* Supplied by the Norton Company.

than two orders of magnitude, compared to the "standard" (HS130) material. This has a profound effect on the life expectancy under stress at high temperatures, as we shall demonstrate later. Conversely, the size and spatial distribution of impurity has no significant effect on the slow crack growth rate. The particulate composites of silicon nitride and silicon carbide exhibit inferior slow crack growth behavior.*

The effects of stress cycling on the crack growth rates are examined next. Slow crack growth rates have been determined for a range of ΔK and $(K_I)_{av}$ and are plotted as a function of $(K_I)_{av}$ at 1400°C in Fig. 7. It is first noted that the cyclic slow crack growth rates are only marginally larger than the static rates. This is exactly what we would expect if the cyclic slow crack growth mechanism is the same as the static mechanism. Quantitative cyclic and static slow crack growth rate correlations, obtained using the Evans and Fuller analysis,[11] are shown in Table II. The predicted crack growth rates are in good agreement with the measured rates. This is a rather unexpected result

---

* However, there may still be advantages to using silicon carbide and silicon nitride composites if the slow crack growth in these materials is accompanied by acoustic emission.[14] This aspect of the failure prediction problem is not dealt with extensively in this paper, but nevertheless, it is an interesting possibility which will be examined and reported in a future publication.

because it is generally found, in metals, that when there is extensive crack tip plasticity, cycling yields crack growth rates substantially larger than the rates expected from the static process.[13] It is noted however that measurements have only been performed at relatively low frequencies, approximately 1 cycle per second or less, and that enhanced effects may exist at larger frequencies. (But the enhanced cycling effects observed in ductile materials show up primarily at the low frequencies;[13] and if an enhanced effect is found for silicon nitride at the higher frequencies it will be due to some process other than the conventional cyclic fatigue process.)

3.2 Alumina

Slow crack growth rate measurements in aluminas at high temperatures[5] are less interesting. Only a relatively narrow (stress intensity factor) range of slow crack growth is observed (Fig. 8), and in contrast to the observations in silicon nitride in region B the critical stress intensity factor diminishes as the temperature is increased.

Acoustic emission measurements have been performed on these materials during high temperature crack propagation (Fig. 8). Only limited information is available at present, but there does appear to be a good correlation between the acoustic emission rate and the slow crack growth rate, consistent with similar measurements performed at room temperature.[5]

The very interesting phenomenon of crack healing has also been examined in alumina at elevated temperatures.[15] Relatively low loads are imposed on precracked double torsion specimens and the rate at which the crack

heals is determined by direct measurement of the crack healing increment in a certain time interval. Only limited information (at 1400°C) is presently available (Fig. 9), but some very interesting features are emerging. Note, especially, that the crack healing rate diminishes very rapidly at quite small stress intensity factors.

3.3 Silicon Carbide

Some very preliminary measurements for slow crack growth have been performed using a recrystallized silicon carbide. For this material, only a limited K_I range of slow crack growth ($K_I > 0.9\ K_{IC}$) is observed even at 1400°C; and both the range of slow crack growth and the critical stress intensity factor are essentially temperature independent. Presumably, rather more interesting slow crack growth behavior will be observed in the hot-pressed silicon carbides. We have not yet attempted to perform measurements on these materials, but studies will be initiated presently.

4. FAILURE PREDICTIONS

4.1 General Failure Time Analysis

The crack growth, and hence the failure time,* can be predicted

---

* These predictions are based on the two premises that failure is primarily propagation controlled (i.e., the flaw initiation time is insignificant) and that the fracture mechanics parameters apply to the relatively small pre-existing flaws that lead to fracture in a typical component. This appears to be justified for silicon nitride,[4] although more work is needed to substantiate this assumption.

from the slow crack growth data, by combining the K_I,v relation (Eq. (3)) with the fracture mechanics relation, $K_I = \sigma Y\sqrt{a}$ (σ is the stress and a is the crack length), to give;

$$V = \frac{da}{dt} = A\sigma^n Y^n a^{n/2}, \tag{4}$$

and then rearranging and integrating to obtain;

$$\int_{a_1}^{a_2} \frac{da}{Y^n a^{n/2}} = A \int_o^t \sigma^n dt \tag{5}$$

Normally, the geometric parameter Y is considered to be constant[6] and taken outside the integral. However, in silicon nitride where slow crack growth occurs over a wide range of stress intensity factors, the crack length at failure is often a significant fraction of the component dimensions.[3] Then it is not valid to consider Y as constant. We shall therefore perform the time-to-failure integration in general form, to evaluate the importance of a variable Y in failure-time predictions. Initially, the integration is conducted at constant stress, and then for a cyclic stress at constant Y. The complete case of variable Y and variable stress can be performed, but only by using numerical methods.

(a) Constant Stress

For constant stress, σ_a, Eq. (5) becomes

$$t = \frac{1}{A\sigma_a{}^n} \int_{a_o}^{a_c} \frac{da}{Y^n a^{n/2}} \tag{6}$$

where a_o is the initial crack length and a_c is the critical crack length for rapid fracture. Inserting the appropriate Y for the test configuration into Eq. (6) enables t to be computed. For example, if we consider a tensile specimen,[7] Y is approximately constant ($\sim$ 2.0) in the range $0 < a/W < 0.2$ (where W is the specimen thickness); but increases for larger a/W, with $Y \approx 10\ a/W$. Hence the time to failure becomes,

$$t \approx \frac{1}{A(\sigma_a)^n 2^n} \int_{a_o}^{0.2W} \frac{da}{a^{n/2}} + \frac{W^n}{A(\sigma_a)^n 10^n} \int_{0.2W}^{a_c} \frac{da}{a^{3n/2}} \tag{7}$$

Integration gives;

$$t = t_o \left\{ 1 - \left(\frac{5a_o}{W}\right)^{\frac{n-2}{2}} \left[1 - \left(\frac{n-2}{3n-2}\right) \right] - \left(\frac{n-2}{3n-2}\right) \left(\frac{a_o}{a_c}\right)^{\frac{n-2}{2}} \left(\frac{W}{5a_c}\right)^n \right\} \tag{8}$$

where t_o is the time to failure for constant Y, given by;

$$t_o = \frac{2}{A(n-2)\sigma_a{}^2 Y^2 K_{Ii}{}^{n-2}} \tag{9}$$

where K_{Ii} is the maximum stress intensity factor on initial loading. It is apparent from Eq. (8) that the crack length at rapid fracture, a_c does not significantly affect the time to failure; in fact, the larger is a_c the closer t comes to t_o (because an increase in a_c implies a decrease in the stress and more of the time is expended at small crack lengths). The corrections due to variable Y only become important when a_o is relatively large ($\tilde{>}$ 0.3W), and this is not the case for typical silicon nitride components. Hence, the simple relation for failure time given by Eq. (9) can be used for failure prediction at constant stress without incurring significant error, even when extensive slow crack growth occurs.

(b) Variable Stress

For a variable stress, $\sigma(t)$, and constant Y, Eq. (5) gives;

$$\int_{a_o}^{a_c} \frac{da}{a^{n/2}} = AY^n \int_o^{t_c} \sigma(t)dt \tag{10}$$

where t_c is the failure time, or,

$$\int_0^{t_c} \sigma(t)dt = \frac{2}{AY^2(n-2)} \left(\frac{\sigma_i}{K_{Ii}}\right)^{n-2} \qquad (11)$$

The left hand integral can be solved using series solutions for various $\sigma(t)$,[11] and the results can be expressed in the form;

$$t_c = g^{-1} t_o \qquad (12)$$

where t_o is the static time to failure at the equivalent <u>average</u> stress and g is a dimensionless quantity which depends on the type of stress cycle, the amplitude of the cycle and n. For example, values of g^{-1} for a sinusoidal cycle are shown in Fig. 10.

4.2 <u>Failure Prediction Techniques</u>

The relations in Eqs. (9) and (11) can be used directly for failure prediction by inserting values for K_{Ii}. This can be achieved either statistically or absolutely.

The statistical result, based on a Weibull distribution function is, for low probabilities[6] ($\lesssim 0.1$);

$$\log t = \frac{(n-2)}{m} \log P - n \log \sigma a + \phi \qquad (13)$$

where m is the shape parameter for the distribution, P is the fracture probability and ϕ is a constant.

For absolute failure predictions some flaw detection procedure must be used. One of the most effective "flaw detection" techniques for ceramic materials is overload proof testing.[6,2,16] A proof test to a stress, σ_p, permits a minimum in-service failure time, t_{min}, to be predicted, given by;[6]

$$t_{min} = \frac{2}{A(n-2)\sigma_a{}^2 Y^2 K_{IC}{}^{n-2}} \left[\left(\frac{\sigma_p}{\sigma_a} \right)^{n-2} - 1 \right] \qquad (14)$$

where K_{IC} is the critical stress intensity factor under the proof test conditions.

The minimum failure time after proof testing is determined directly from the slow crack growth data, and the statistical distribution of times is obtained from the slow crack growth data in conjunction with strength data (determined in the absence of slow crack growth, i.e., at room temperature for silicon nitride). Both failure time solutions can be plotted on the same diagram to obtain a complete picture of the structural capabilities of the material.

4.3 Application

The failure prediction analysis developed above is now applied to the silicon nitride data to evaluate the performance capabilities of the various compositions. First, the proof stress diagrams for room temperature proof testing and a 1400°C operating temperature are evaluated for two proof stress ratios; 2 to 1 and 6 to 1. These are shown in Fig. 11. First, it is noted that a substantial discrepancy emerges when comparing failure predictions (for the standard material) obtained using the old data (Fig. 3) with the predictions from the new data (Fig. 5). The discrepancy is due, of course, to the lack of low velocity data in the former and re-emphasizes the crucial importance of low velocity data for failure prediction. The higher purity materials exhibit substantially longer failure times, by about two orders of magnitude; for example, a proof stress ratio of 6 to 1 ensures failure times > 1 yr for stresses < 10 MNm^{-2}.

The statistically related failure times are estimated for the higher purity materials from four-point flexural strength data obtained at room temperature.[10] The strength data relate to the standard material and it is assumed that comparable room temperature strengths can be obtained for the higher purity materials. The strength data exhibit a reasonable fit to an assumed Weibull distribution, giving a zero location parameter and a value for m = 8. The corresponding failure times at 1400°C computed using Eq. (13) are shown in Fig. 12 for the probabilities 10^{-1}, 10^{-3}, and 10^{-5}. Also shown in the diagram are approximate failure times in tension,

for $P = 10^{-5}$, assuming that the tensile strength is approximately half the flexural strength.

Let us now consider the maximum operational stresses that this material can be subjected to, at 1400°C. If we take 1 yr ($\sim$ 10,000 hrs) as a useful life expectancy, and consider that the component has a median strength about half the median flexural strength, then we see from Fig. 12 that the stress levels corresponding to fracture probabilities of 10^{-5}, 10^{-3} and 10^{-1} without proof testing are 12, 20 and 30 MNm^{-2}, respectively. Alternatively, a failure time of 1 yr is assured at 30 MNm^{-2} by proof testing at a 9 to 1 proof stress ratio, i.e., 270 MNm^{-2}. (This is, of course, a very large proof stress ratio which may well be impractical.) The maximum stress capability of this material may thus be taken as 30 MNm^{-2} at 1400°C. This may suffice in some applications, but additional improvements are evidently desirable. For example, an improvement comparable to that achieved from the standard to the higher purity material discussed here would be sufficient for many applications.

Finally, it is noted that the material exhibits substantially improved strength capabilities at lower temperatures. For example, decreasing the temperature by 100°C to 1300°C gives a 10,000 hr strength more than 5 times the strength at 1400°C, i.e., > 150 MNm^{-2}.

5. MECHANISMS

Elevated temperature slow crack growth processes in ceramic materials are primarily independent of environment. The slow crack growth mechanisms

are mostly related to crack tip plasticity,* (which occurs in these materials at high temperatures). Two distinct plasticity-related slow crack growth processes can occur in ceramic materials (although it is noted that additional mechanisms are possible in ductile systems), due to two different modes of plasticity; dislocation motion and grain boundary sliding. Models describing slow crack growth under these conditions are developed, but only in a semi-quantitative fashion, noting that fracture is predominantly intergranular.

5.1 Dislocation Assisted Slow Crack Propagation

The model for the dislocation-related process is depicted schematically in Figure 13. In polycrystalline ceramics, grain boundaries are frequent sources of dislocations, particularly in the oxide ceramics and alkali halides. Hence, we envisage that when a stress is applied to a cracked body, the stresses in the vicinity of the crack tip will cause dislocations to be emitted from nearby grain boundary sources (S in Fig. 13). These dislocations will glide along their slip planes and pile up at the opposite grain boundary (X in Fig. 13). The details of the dislocation transmission across the grains are rather complex, due to the undulations of the crack tip shear stress field. However, detailed

---

* A possible alternative mechanism for the alumina is vacancy condensation at the crack;[17] but this process is not examined in this paper for conciseness of presentation.

examination of these stress fields[18] shows that the process depicted in Fig. 13 is expected for most grain orientations (depending on the slip systems). The dislocation pile up initiates a grain boundary crack (in the Stroh sense), this links with the primary crack, and hence produces the crack length increment which constitutes the slow crack growth. A very simple analysis which identifies the important crack propagation parameters for this process is conceived as follows:

If we consider that the dislocations move across the grain at a stress equivalent to the average shear stress acting along the plane, $\bar{\tau}$, then the number of dislocations that form the pile up, η, is given by;[19]

$$\eta = \frac{\ell(\bar{\tau}-\tau_o)}{\mu b} \qquad (15)$$

where ℓ is the length of the pile-up (G, the grain size), τ_o is the friction force opposing dislocation motion, μ is the shear modulus and b the Burgers' vector for the dislocations. The number of dislocations in the pile up determines the tensile stress at the tip of the pile up[19] ($\sigma_{tip} = \eta(\bar{\tau}-\tau_o)$). Once this exceeds the theoretical strength of the material, a grain boundary crack will form at the end of the pile up. Putting the condition, therefore, that the stress at the tip of the pile up is equivalent to the theoretical strength[20] ($\sigma_{tip} \approx \sqrt{E\gamma/C_o}$) gives;

$$\bar{\tau} = \tau_o + \left(\frac{\mu b}{\ell}\right)^{\frac{1}{2}} \left(\frac{E\gamma}{C_o}\right)^{\frac{1}{4}} \qquad (16)$$

where c_o is the lattice parameter, E is Young's modulus and γ is the grain boundary fracture energy. The shear stress along the slip plane is clearly dependent on the stress intensity factor and is given by;[21]

$$\tau = \frac{K_I}{\sqrt{2\pi r}} \; f(\theta), \qquad (17)$$

where r is the distance from the crack tip and $f(\theta)$ is the angular dependence of τ. Combining Eqs. (16) and (17) gives the stress intensity factor required to initiate a secondary crack, due to the dislocation pile up;

$$K_I = B\tau_o\sqrt{\ell} + B' \left(\frac{b^2\gamma}{c_o}\right)^{\frac{1}{4}}, \qquad (18)$$

where B and B' are constants. Generally, when a crack is initiated at the tip of a pile up, the crack will propagate to a size substantially larger than the pile up length.[22] We expect therefore that the stress intensity given by Eq. (18) is also sufficient for the secondary crack to link with

the primary crack; hence, the condition for propagation of the primary crack along one grain boundary has been obtained.

We can further extend the model by noting that the lattice resistance to dislocation motion is a function of both the dislocation velocity, v, and the temperature;[23]

$$v = A'\tau^{m^*}f(T) \tag{19}$$

where A' is a constant and m* is the strain rate sensitivity. If we now combine this relation with Eq. (18), we obtain a relation between K and crack velocity which suggests that the slow crack growth rate is controlled by the dislocation strain-rate sensitivity exponent, i.e., $n \approx m^*$. Hence, a good test of the model is a comparison of measured values of n and m*. The existing data on alumina (which might exhibit this mode of slow crack growth) is unfortunately rather limited and it is not useful to make direct quantitative comparison, but the trends are quite consistent with this model; i.e., both n and m* are large[24] and the K_I range in which slow crac growth occurs is small. We await more detailed empirical evaluation of slow crack growth rates for quantitative comparison with the model.

5.2 Grain Boundary Sliding Induced Slow Crack Growth

Slow crack growth can also occur due to grain boundary sliding near the crack tip. A model for this process that applies to materials

with rigid grains and a narrow viscous grain boundary phase (typifying the grain boundary sliding process in silicon nitride) is depicted schematically in Fig. 14. Analysis of this process presents several formidable problems and a complete analysis has not yet been developed. The sequence of events is as follows:

Sliding occurs along the grain boundary (AB) adjacent to the crack tip. Using Eq. (17) in conjunction with the stress dependence of the sliding rate ($\dot{\delta} \alpha \sigma^N$, where $N \approx 1$), the displacement, δ, that occurs in time, t, can be obtained;[25]

$$\delta = k \left[\left(\frac{2G}{\pi} \right)^{\frac{1}{2}} K_I f(\theta) \right]^N t \qquad (20)$$

where k is the proportionality in the sliding rate relation. This displacement is transferred by the rigid grains to the triple point at B, and a grain size crack will form from B, along the grain boundary (BC), when δ reaches a critical value, δ_c. The crack at BC enhances the stress at the primary crack tip, but only by a small amount* ($\tilde{<}$ 10%). Hence in the range

---

* A detailed analytical solution for the stress intensification is not available, but the solution for two equivalent size cracks can be used to estimate the order of the effect.[26] Also a simplified analysis assuming non-interacting cracks can be used and this gives a similar result.

$0.9\ K_{IC} < K_I < K_{IC}$ the formation of this secondary crack may induce separation along AB and the primary crack will move forward, due to this event, by $\sim 3/2\ G$. The V, K_I relation in this range is thus obtained from Eq. (20) and is given by;

$$V = \frac{Gk}{\delta_c} \left[\left(\frac{2\pi}{G} \right)^{\frac{1}{2}} f(\theta) \right]^N K_I^N \qquad (21)$$

It is also noted at this stage that K_{IC} corresponds to fracture by grain separation (opening) at A and will occur when δ, at A, is δ_c. The increase in K_{IC} in silicon nitride with increase in temperature is thus accounted for by an increase in δ_c due to a decrease in the viscosity of the grain boundary phase.

At lower K_I, separation along AB can no longer occur and sliding now commences along CD due to the formation of the secondary crack. The rate of sliding here can be obtained by summing the shear stresses along CD due to the primary crack and the wedge opening of the secondary crack (due to the sliding along AB). The stress intensity factor at C due to the wedge opening at B can be obtained from Barenblatt's wedging analysis,[27] and in its simplest form the solution is;

$$K_I = \frac{E\delta}{2(1-\nu^2)\sqrt{G}} \qquad (22)$$

The sliding displacement along CD due to the total K_I at C can thus be found in the exact manner used to derive Eq. (20). Putting the displacement equal to δ_c then gives the condition for forming another secondary crack along DE, which further enhances the stress at the primary crack tip. This process can be continued until a large zone of subsidiary microcracks is developed, and the corresponding K_I at the primary crack evaluated. The analysis has not yet been completed, but the important trends are emerging. Notably, the crack growth rate will be a function of K_I and the grain boundary sliding rate-constant, and hence qualitatively consistent with the slow crack growth observations.

6. SUMMARY

Slow crack growth has been examined in several systems at elevated temperatures. The double torsion specimen has been identified as an appropriate specimen for fracture mechanics measurements at high temperatures, but with the use mode (fixed grips, constant displacement rate, fixed load) depending on the extent of the accompanying plasticity.

Data obtained for silicon nitride, silicon carbide and alumina have been examined, and these show that purity plays a major role in controlling the slow crack growth resistance. Crack growth rate data evaluated for silicon nitride under cyclic loading conditions show the unexpected result, that cycling does not enhance the crack growth rate at low frequencies, even though substantial crack tip plasticity is occurring.

Failure prediction analyses have been presented which enable failure times to be evaluated from the fracture mechanics data. Two types of failure prediction have been emphasized; a statistical prediction based on the initial strength distribution, and an absolute prediction for the minimum failure time after proof testing. The silicon nitride data have been transformed into failure diagrams (containing these predictions) which may be used for design purposes or for materials evaluation.

Finally, models for the plasticity related slow crack growth process which may occur in ceramic materials at elevated temperatures have been described. The models are not fully quantitative, as yet, but they demonstrate the important parameters controlling the rates of slow crack growth.

REFERENCES

1. S. M. Wiederhorn, Fracture Mechanics of Ceramics, to be published.
2. A. G. Evans and T. G. Langdon, Structural Ceramics, Progress in Materials Science, to be published.
3. F. F. Lange, J. Am. Ceram. Soc., to be published.
4. A. G. Evans and S. M. Wiederhorn, J. Mater. Sci., to be published.
5. A. G. Evans, M. Linzer and L. R. Russell, Mater. Sci. Eng., to be published.
6. A. G. Evans and S. M. Wiederhorn, NBSIR 73-147, March 1973; Int. J. Frac., to be published.
7. A. G. Evans, Fracture Mechanics of Ceramics, to be published.
8. D. P. Williams and A. G. Evans, J. of Testing and Evaluation, 1, 264 (1973).
9. A. G. Evans, J. Mater. Sci. 7, 1137 (1972).
10. A. G. Evans, L. R. Russell and D. W. Richerson, to be published.
11. A. G. Evans and E. R. Fuller, Met. Trans., January 1974, to be published.
12. F. F. Lange, unpublished work performed at Westinghouse Research Laboratories.
13. See for example: Corrosion Fatigue, NACE Publication (Ed. O. F. Deveraux, A. J. McEvily, R. W. Staehle), 1972.
14. A. S. Tetelman and A. G. Evans, Fracture Mechanics of Ceramics, to be published.

15. A. G. Evans and L. R. Russell, to be published.

16. A. G. Evans, J. Mat. Sci., to be published.

17. R. M. Stephens and R. Dutton, Mater. Sci. Eng. 8, 220 (1971).

18. R. M. Thomson and A. G. Evans, to be published.

19. J. P. Hirth and J. Lothe, Theory of Dislocations (McGraw Hill, New York), 1968.

20. A. Kelly, Strong Solids, (Clarendon, Oxford) 1966.

21. P. C. Paris and G. C. Sih, ASTM STP 381 (1967) p. 30.

22. A. N. Stroh, Advances in Physics 6, 418 (1957).

23. A. G. Evans and R. D. Rawlings, Phys. Stat. Sol., 34, 9 (1969).

24. H. Conrad, G. Stone and K. Janowski, Met. Trans., 233, 889 (1965).

25. A. G. Evans, to be published.

26. M. Isida, Methods of Analysis and Solutions of Crack Problems (Ed. G. C. Sih, Noordhoff, 1973), p. 121.

27. G. I. Barenblatt, Advances in Applied Mechanics, 7, (1962).

TABLE I

SILICON NITRIDES CLASSIFICATION

Materials		Relative Deleterious Impurity Content	Impurity Distribution
Standard	Type I	1	Wide Inclusion Size Distribution
	Type II	1	Narrow Inclusion Size Distribution
High Purity	Type I	0.2	
	Type II	0.3	
Composites: SiC/Si_3N_4	30/70	> 3	

TABLE II

CYCLIC/STATIC SLOW CRACK GROWTH COMPARISON

	Velocity Ratio (q)	
$\Delta K/(K_I)_{av}$	Predicted	Measured
0.2	1.8	1.5
0.3	3.2	3.0
0.4	6.5	7.0

FIGURE CAPTIONS

Fig. 1. The double torsion specimen.

Fig. 2. The load, displacement behavior observed in a double torsion specimen loaded at constant displacement rate, $\dot{y}$.

Fig. 3. Slow crack growth measurements in "standard" (HS 130 type) hot pressed silicon nitride at various temperatures, using the constant $\dot{y}$ approach.

Fig. 4. Slow crack growth in several silicon nitrides at 1400°C; C is a SiC/Si_3N_4 particulate composite, S is "standard" (HS 130 type) material and HP is a research grade high purity material.

Fig. 5. The same data as in Fig. 4, but plotted using a logarithmic K_I axis, indicating the good fit of all the data to the relation: $V = AK_I^n$.

Fig. 6. Crack growth rates in "standard" silicon nitride in the "strong" (containing hot pressing direction) and "weak" (orthogonal to hot pressing direction) planes, at 1400°C.

Fig. 7. Slow crack growth rates for "standard" material under cyclic loading conditions, plotted against the average K_I for the cycle, $(K_I)_{av}$, for various ratios of $\Delta K/(K_I)_{av}$ at 1400°C.

Fig. 8. Slow crack growth rates and acoustic emission rates in "lucalox" alumina at elevated temperatures.

Fig. 9. Crack healing rates, vs. K_I, in lucalox alumina at 1400°C.

Fig. 10. The g parameter for a sinusoidal stress cycle, for various n and stress amplitudes.[11]

Fig. 11. A proof stress diagram for "standard" and high purity silicon nitrides for proof testing at room temperature and in-service at 1400°C.

Fig. 12. Probability related failure times for failure in flexure and in tension for various probability levels for high purity silicon nitride at 1400°C; also shown are the proof test predictions from Fig. 11.

Fig. 13. A schematic of dislocation assisted slow crack growth in polycrystalline ceramics.

Fig. 14. A schematic of grain boundary sliding induced slow crack growth.

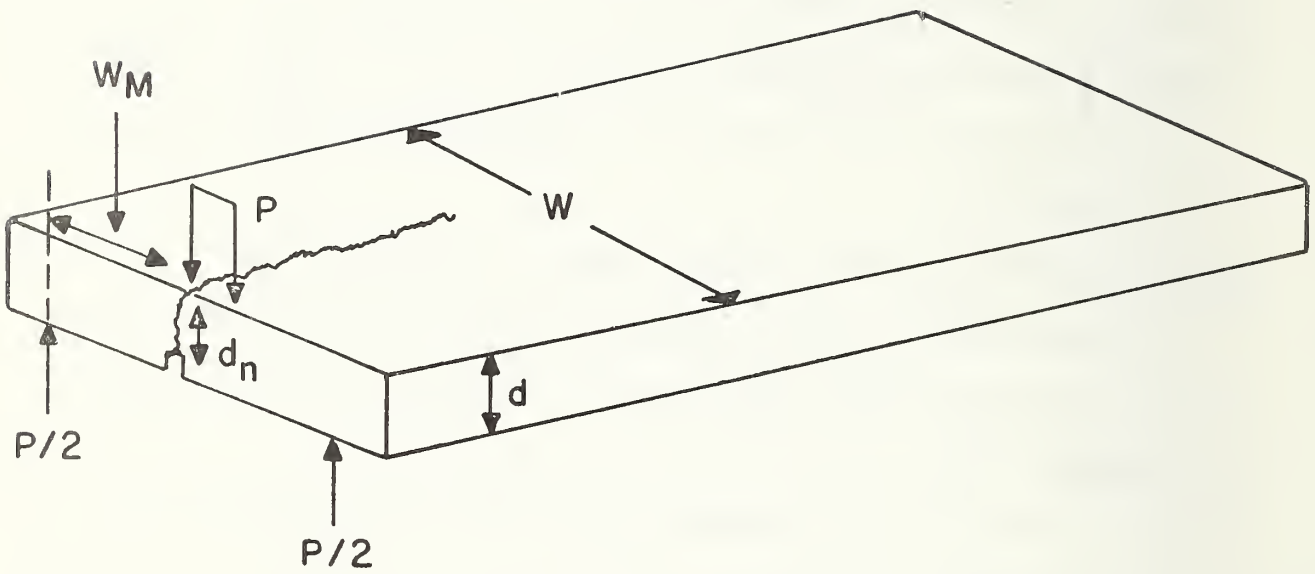

Fig. 1. The double torsion specimen.

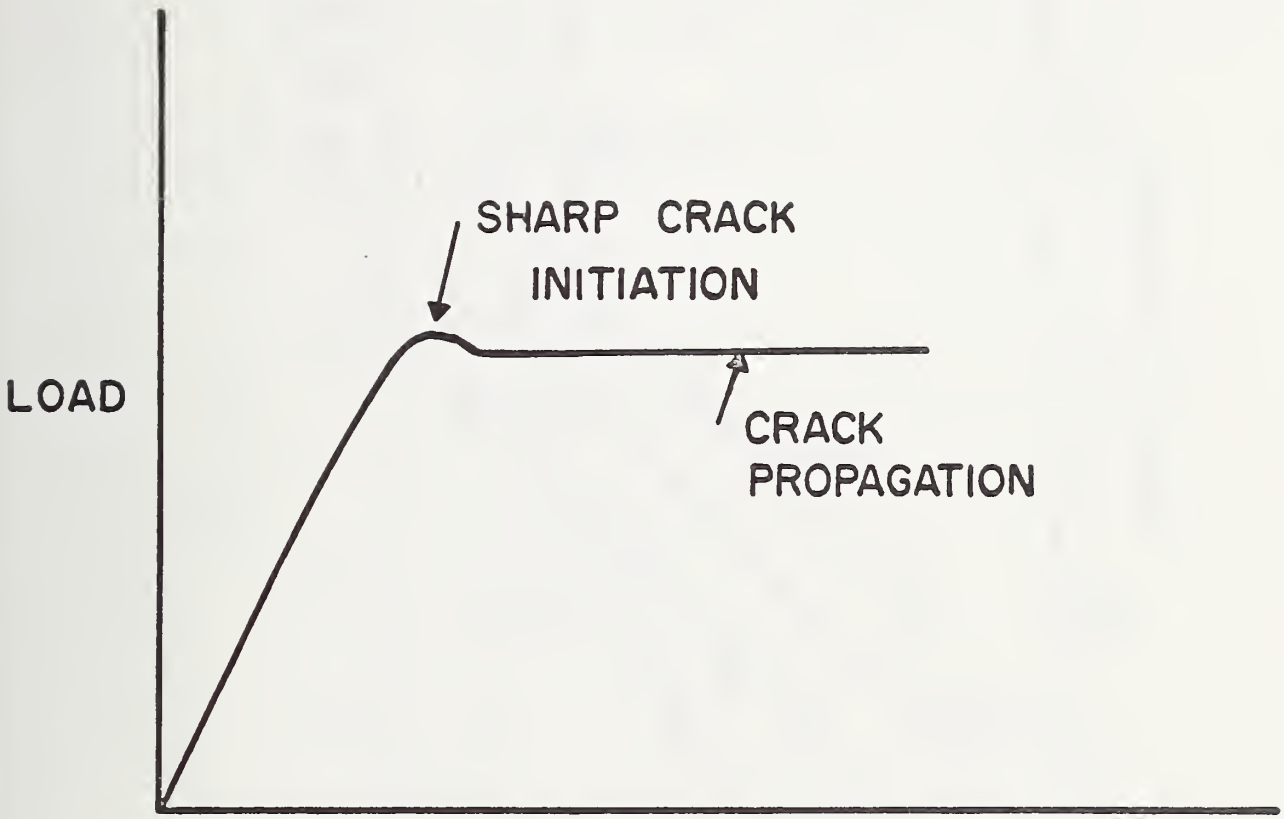

Fig. 2. The load, displacement behavior observed in a double torsion specimen loaded at constant displacement rate, $\dot{y}$.

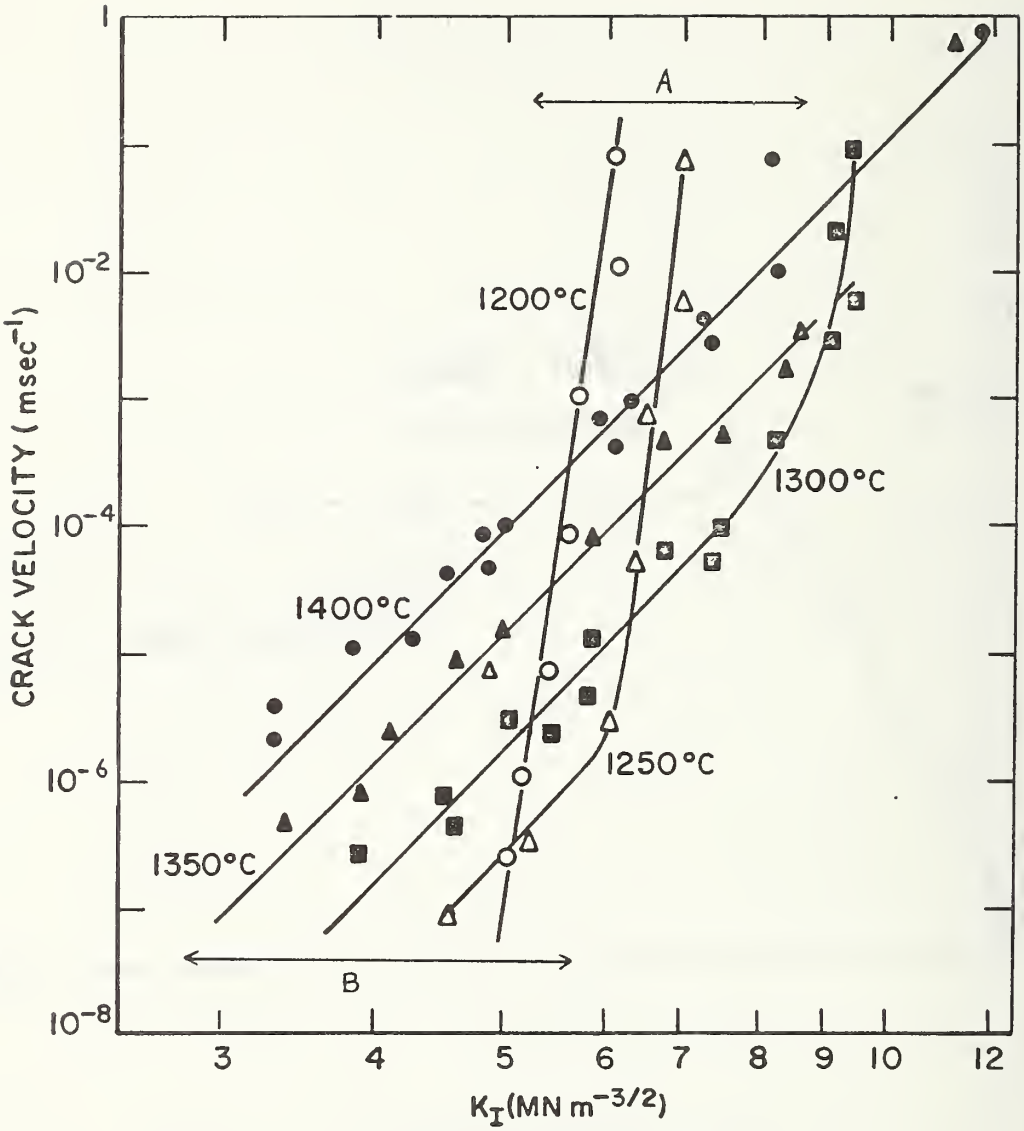

Fig. 3. Slow crack growth measurements in "standard" (HS 130 type) hot pressed silicon nitride at various temperatures, using the constant $\dot{y}$ approach.

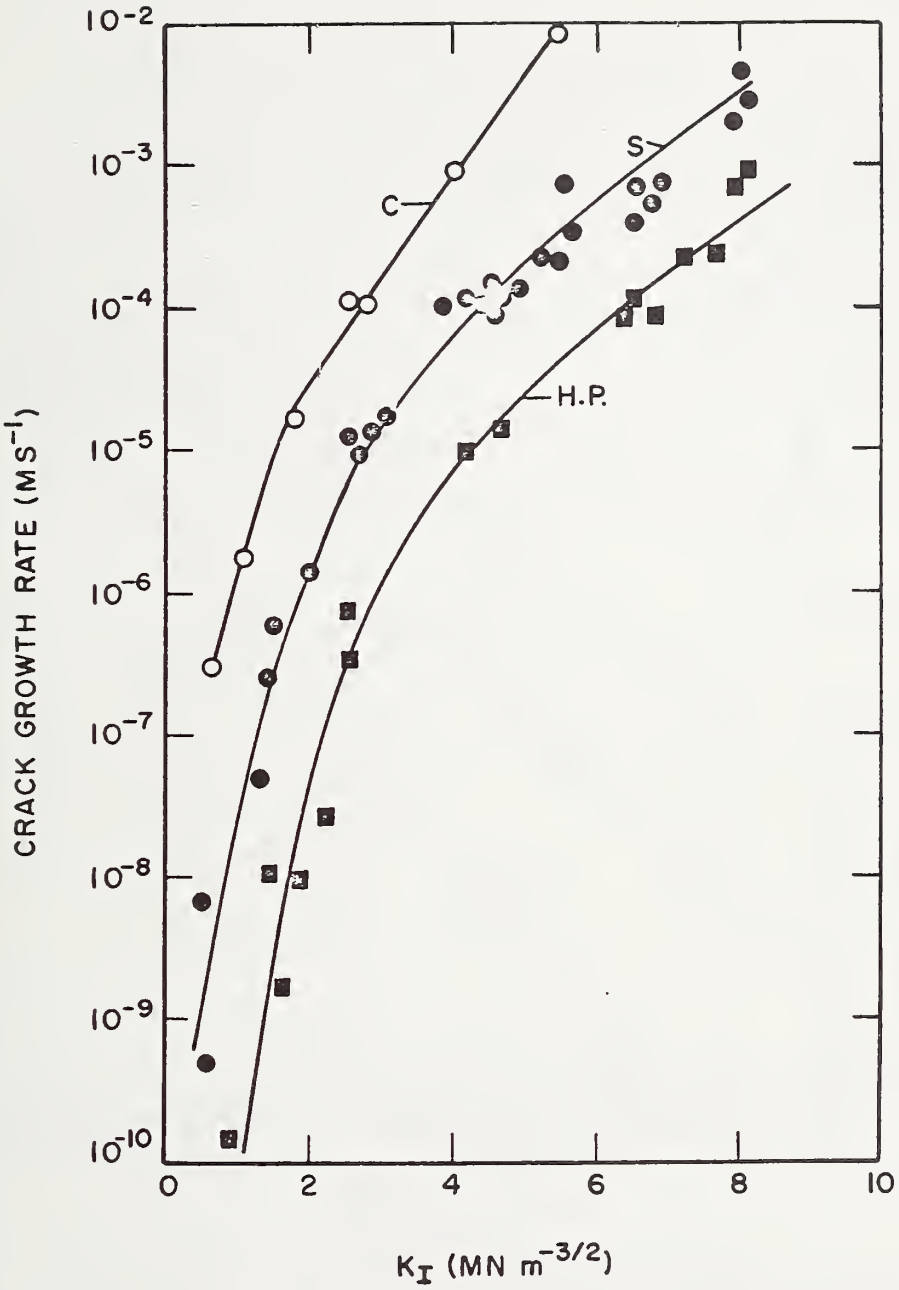

Fig. 4. Slow crack growth in several silicon nitrides at 1400°C; C is a SiC/Si_3N_4 particulate composite, S is "standard" (HS 130 type) material and HP is a research grade high purity material.

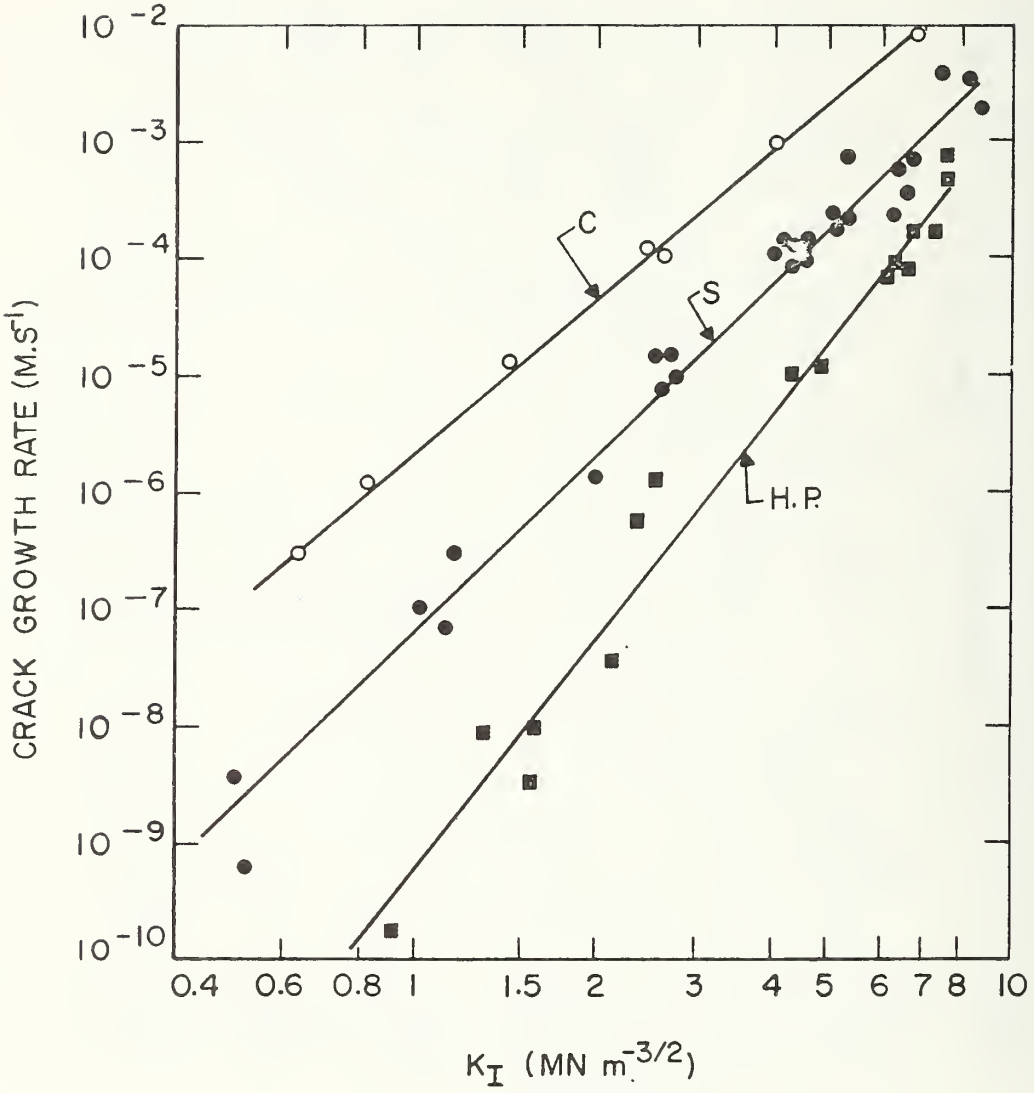

Fig. 5. The same data as in Fig. 4, but plotted using a logarithmic K_I axis, indicating the good fit of all the data to the relation: $V = AK_I^n$.

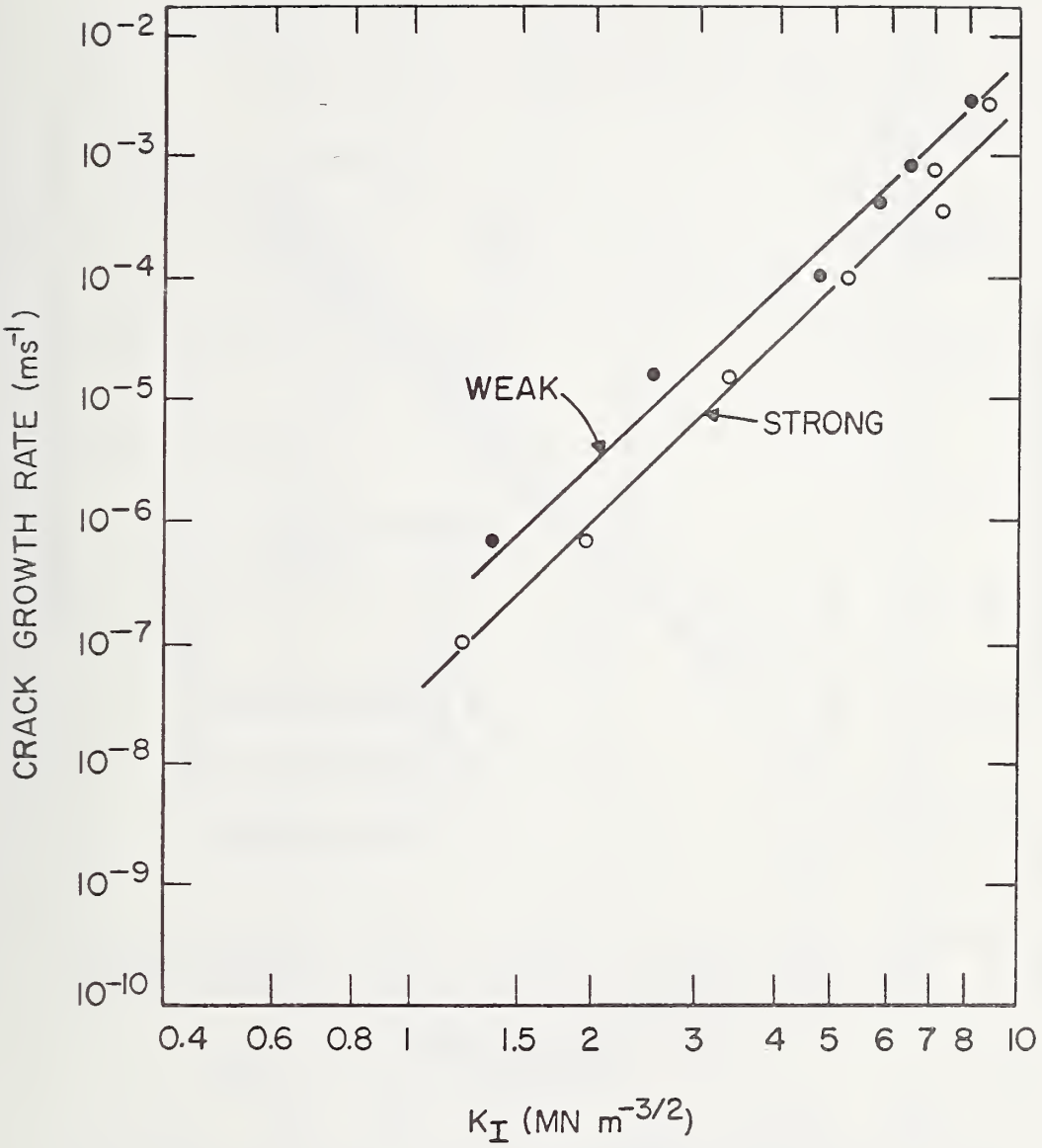

Fig. 6. Crack growth rates in "standard" silicon nitride in the "strong" (containing hot pressing direction) and "weak" (orthogonal to hot pressing direction) planes, at 1400°C.

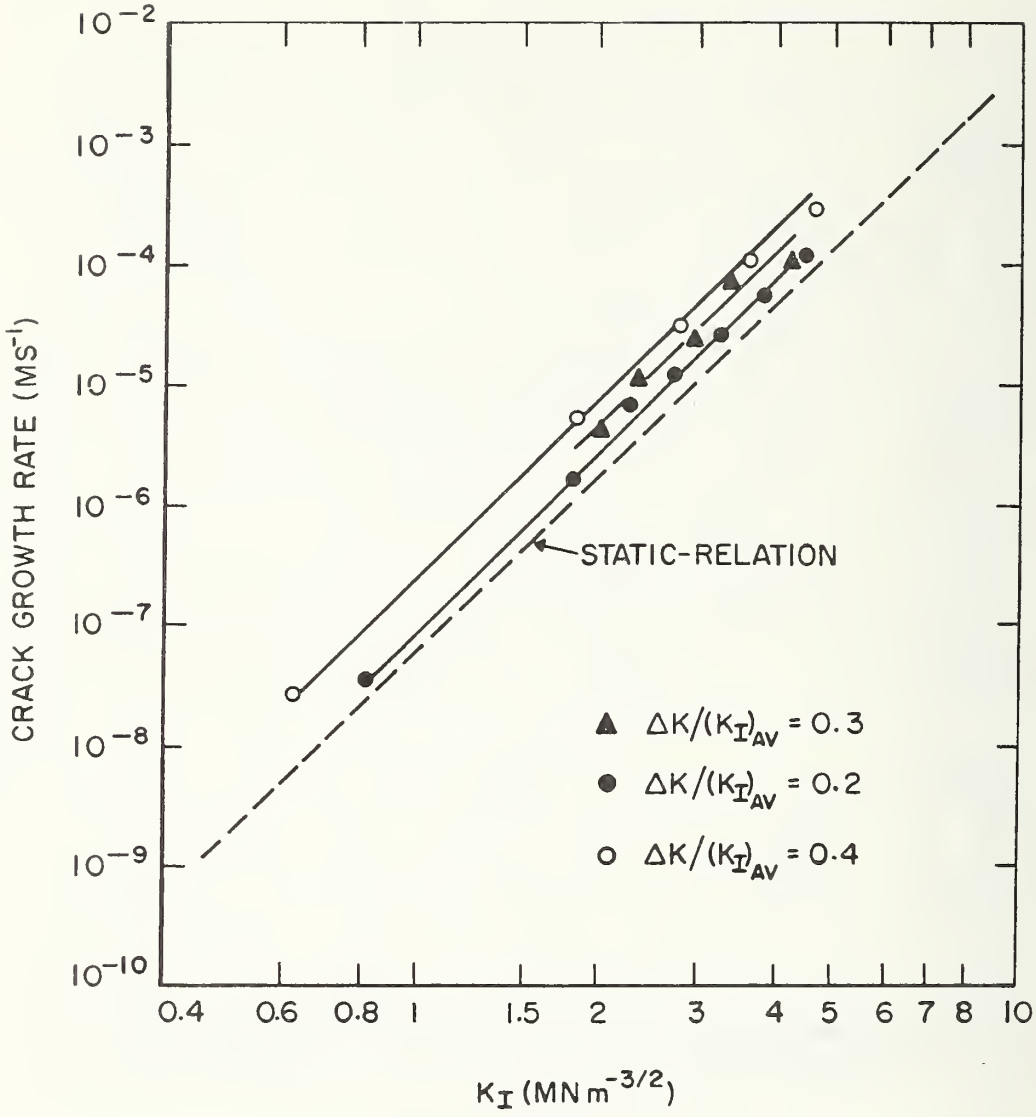

Fig. 7. Slow crack growth rates for "standard" material under cyclic loading conditions, plotted against the average K_I for the cycle, $(K_I)_{av}$, for various ratios of $\Delta K/(K_I)_{av}$ at 1400°C.

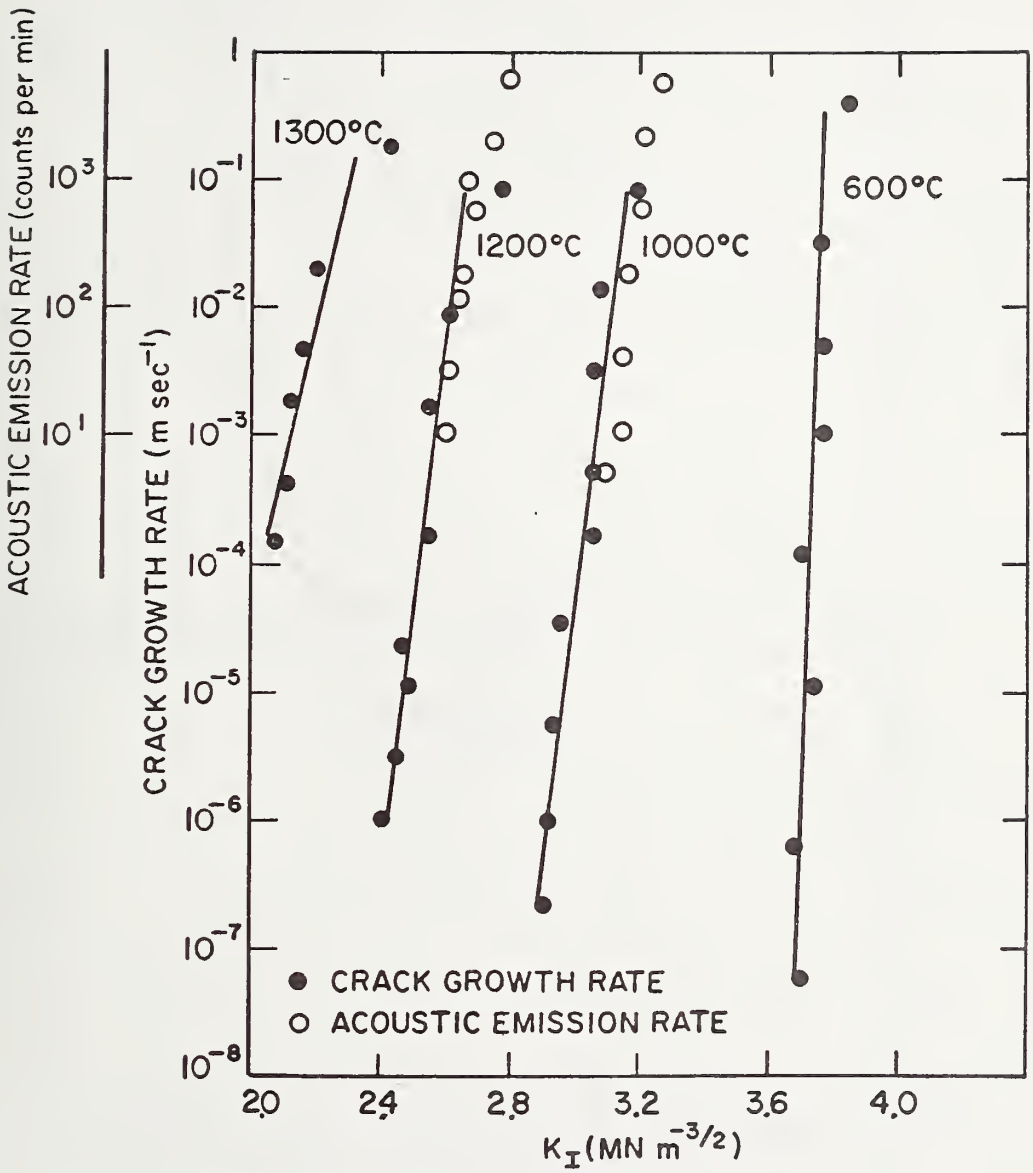

Fig. 8. Slow crack growth rates and acoustic emission rates in "lucalox" alumina at elevated temperatures.

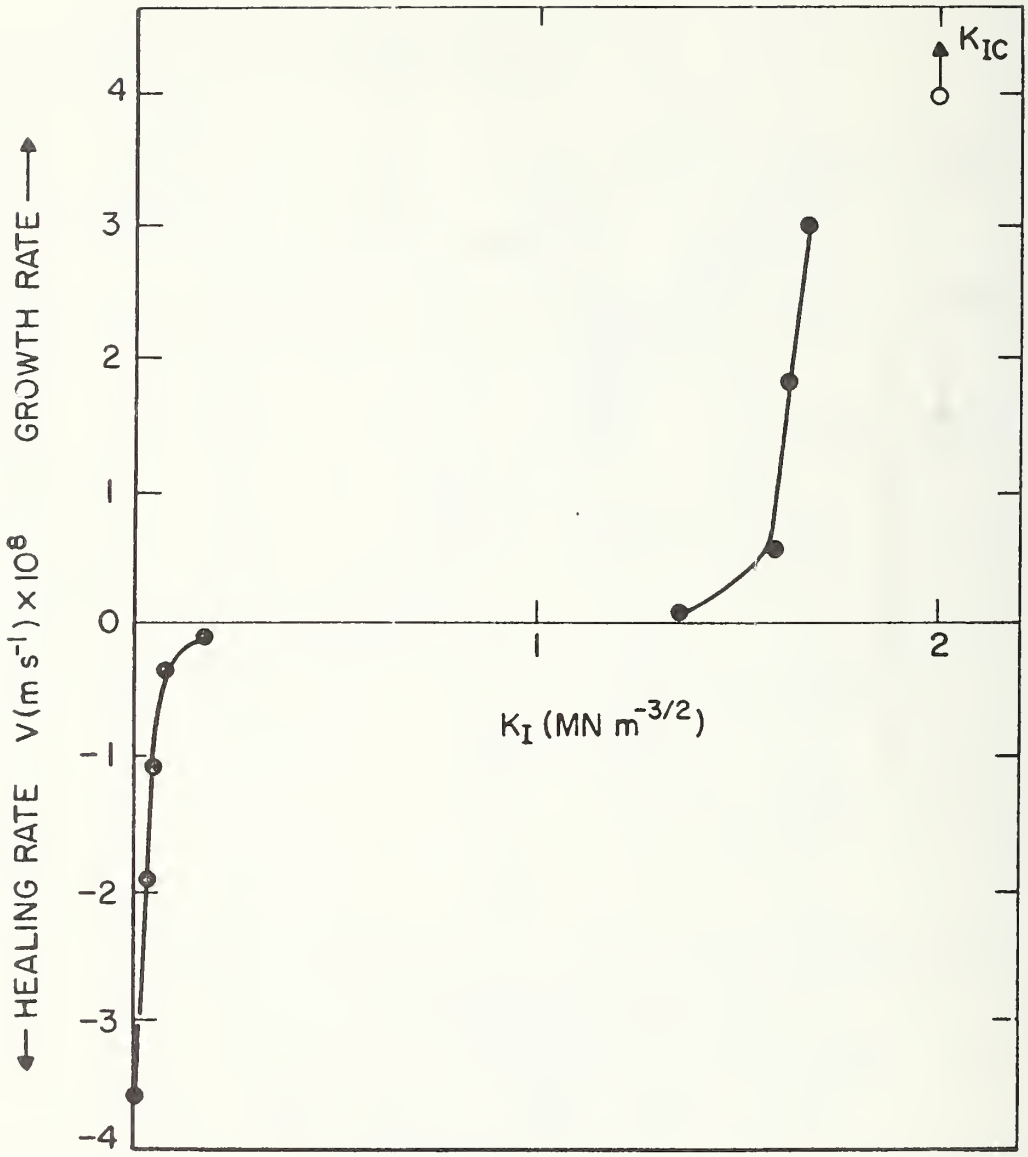

Fig. 9. Crack healing rates, vs. K_I, in lucalox alumina at 1400°C.

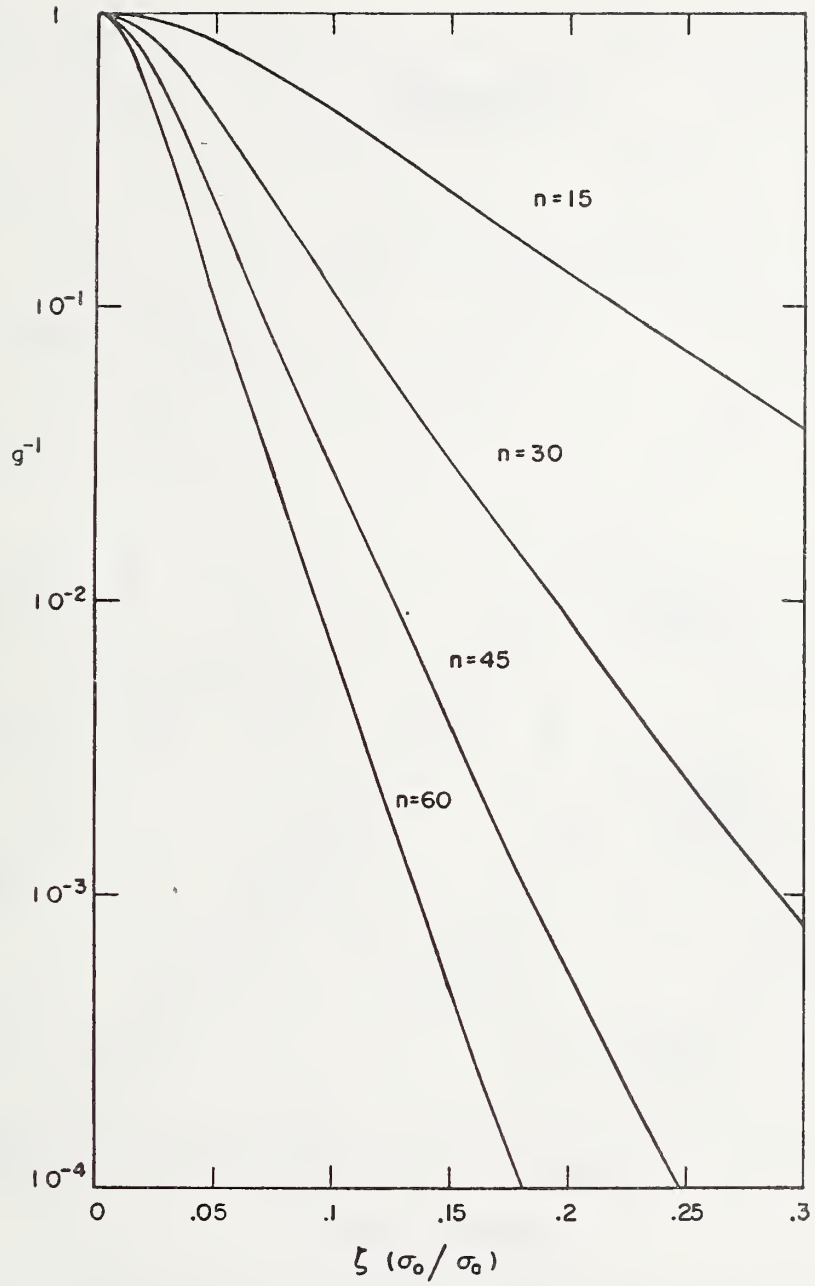

Fig. 10. The g parameter for a sinusoidal stress cycle, for various n and stress amplitudes.[11]

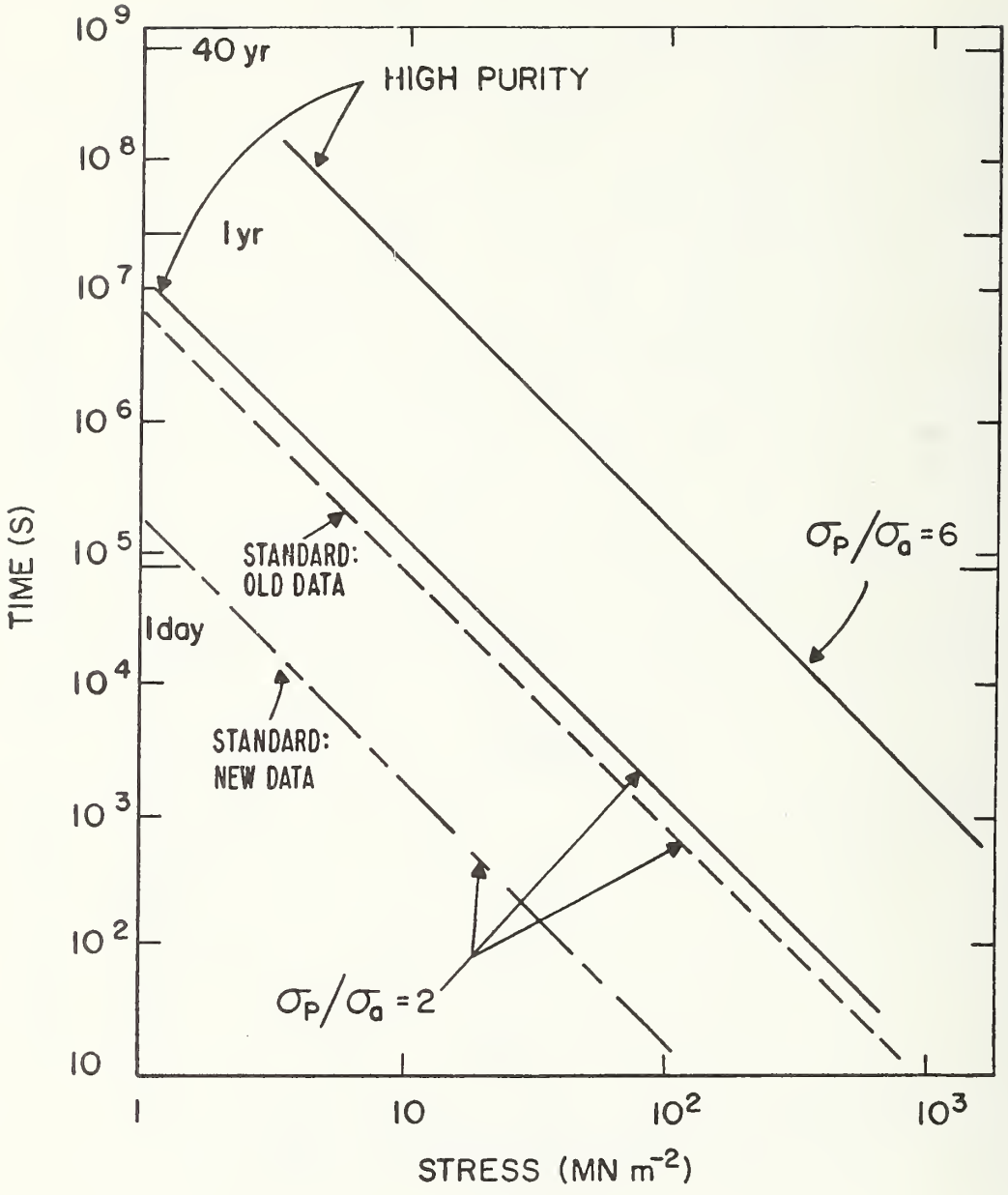

Fig. 11. A proof stress diagram for "standard" and high purity silicon nitrides for proof testing at room temperature and in-service at 1400°C.

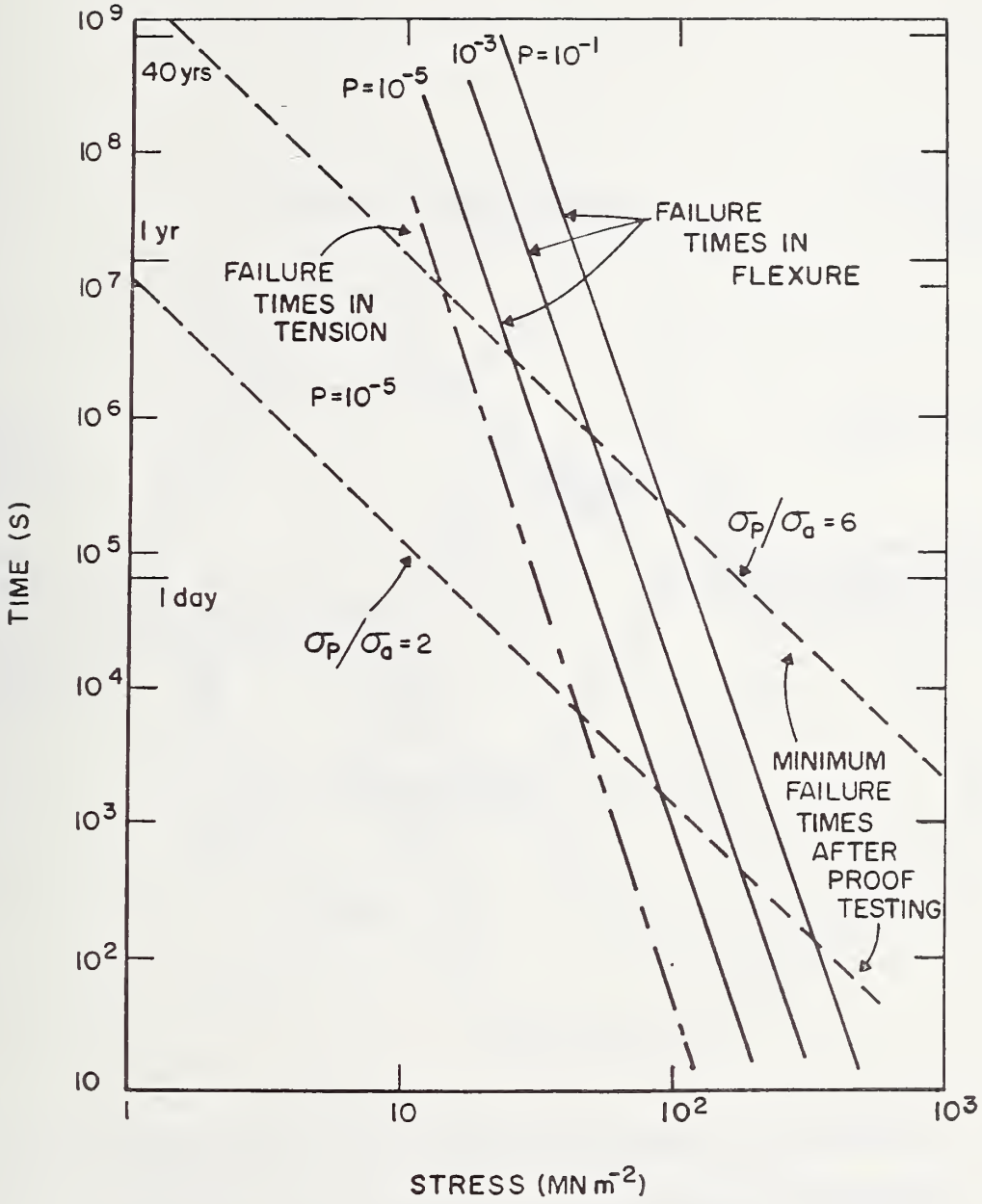

Fig. 12. Probability related failure times for failure in flexure and in tension for various probability levels for high purity silicon nitride at 1400°C; also shown are the proof test predictions from Fig. 11.

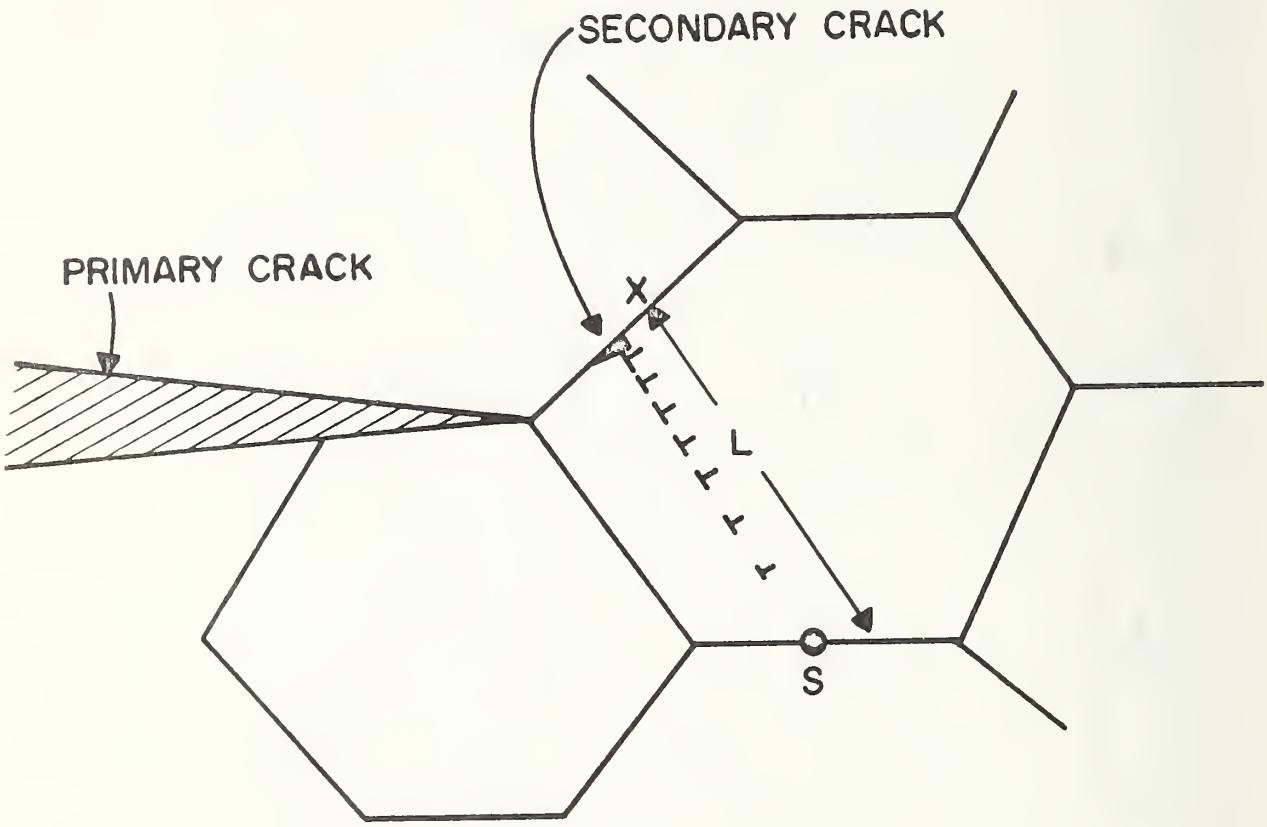

Fig. 13. A schematic of dislocation assisted slow crack growth in polycrystalline ceramics.

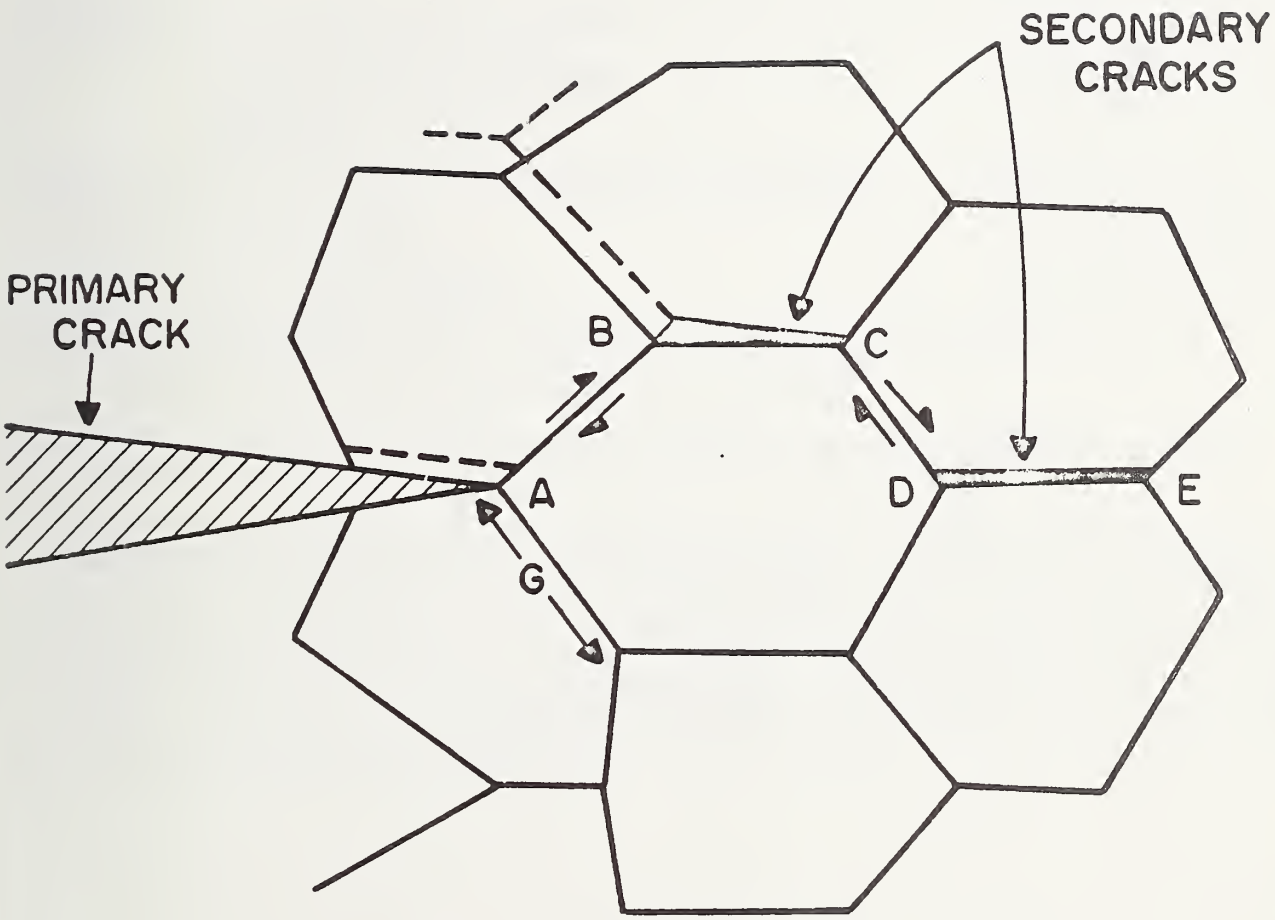

Fig. 14. A schematic of grain boundary sliding induced slow crack growth.

NBS-114A (REV. 7-73)

U.S. DEPT. OF COMM. BIBLIOGRAPHIC DATA SHEET	1. PUBLICATION OR REPORT NO. NBSIR 74-442	2. Gov't Accession No.	3. Recipient's Accession No.

4. TITLE AND SUBTITLE

High Temperature Slow Crack Growth in Ceramic Materials

5. Publication Date February 1974

6. Performing Organization Code

7. AUTHOR(S)

A. G. Evans

8. Performing Organ. Report No. NBSIR 74-442

9. PERFORMING ORGANIZATION NAME AND ADDRESS

NATIONAL BUREAU OF STANDARDS
DEPARTMENT OF COMMERCE
WASHINGTON, D.C. 20234

10. Project/Task/Work Unit No. 3130459

11. Contract/Grant No. F 33615-73-M-6501

12. Sponsoring Organization Name and Complete Address (Street, City, State, ZIP)

United States Air Force
Air Force Systems Command
HQ 4950th Test Wing, 4950/PMMA
Wright-Patterson AFB, Ohio 45433

13. Type of Report & Period Covered Interim
9-1-73 - 1-31-74

14. Sponsoring Agency Code

15. SUPPLEMENTARY NOTES

Also to be published in the Proceedings of Conference on Ceramics for High Performance Applications, Hyannis, Mass., 11/13-16/73.

16. ABSTRACT *(A 200-word or less factual summary of most significant information. If document includes a significant bibliography or literature survey, mention it here.)*

High temperature slow crack growth processes in several ceramic materials are examined under static and cyclic loading conditions. Data obtained at temperatures up to 1400° C are used for purposes of failure prediction and for analysis of the slow crack growth phenomena. It is shown that purity plays a major role in slow crack growth resistance, particularly in the hot pressed materials, and that cycling in the low frequency regime does not significantly increase the rate of slow crack growth. The slow crack growth mechanisms appear to be primarily plasticity related. Two semi-quantitative mechanisms are presented, one due to dislocation motion and the other due to grain boundary sliding.

17. KEY WORDS *(six to twelve entries; alphabetical order; capitalize only the first letter of the first key word unless a proper name; separated by semicolons)*

Ceramics; crack healing; crack propagation; cyclic fatigue; failure prediction; high temperature; static fatigue.

18. AVAILABILITY

[X] Unlimited

[ ] For Official Distribution. Do Not Release to NTIS

[ ] Order From Sup. of Doc., U.S. Government Printing Office Washington, D.C. 20402, SD Cat. No. C13

[ ] Order From National Technical Information Service (NTIS) Springfield, Virginia 22151

19. SECURITY CLASS (THIS REPORT) UNCLASSIFIED

21. NO. OF PAGES 46

20. SECURITY CLASS (THIS PAGE) UNCLASSIFIED

22. Price


AMERICAN REVOLUTION BICENTENNIAL
1776-1976